Research Article | Vol. 28, No. 24 / 23 November 2020 / Optics Express 36632
Optics EXPRESS

Mid-IR refractive index sensor for detecting proteins employing an external cavity quantum cascade laser-based Mach-Zehnder interferometer

ALICJA DABROWSKA,[1] ANDREAS SCHWAIGHOFER,[1,2] STEFAN LINDNER,[1] AND BERNHARD LENDL[1,3]

[1]Institute of Chemical Technologies and Analytics, Vienna University of Technology, Getreidemarkt 9/164-UPA, 1060 Vienna, Austria
[2]andreas.schwaighofer@tuwien.ac.at
[3]bernhard.lendl@tuwien.ac.at

Abstract: Novel laser light sources in the mid-infrared region enable new spectroscopy schemes beyond classical absorption spectroscopy. Herein, we introduce a refractive index sensor based on a Mach-Zehnder interferometer and an external-cavity quantum cascade laser that allows rapid acquisition of high-resolution spectra of liquid-phase samples, sensitive to relative refractive index changes down to 10^{-7}. Dispersion spectra of three model proteins in deuterated solution were recorded at concentrations as low as 0.25 mg mL^{-1}. Comparison with Kramers-Kronig-transformed Fourier transform infrared absorbance spectra revealed high conformance, and obtained figures of merit compare well with conventional high-end FTIR spectroscopy. Finally, we performed partial least squares-based multivariate analysis of a complex ternary protein mixture to showcase the potential of dispersion spectroscopy utilizing the developed sensor to tackle complex analytical problems. The results indicate that laser-based dispersion sensing can be successfully used for qualitative and quantitative analysis of proteins.

1. Introduction

Mid-infrared (mid-IR) spectroscopy (400–4000 cm^{-1}) is an important analytical technique widely used in a variety of scientific fields. It allows for rapid, label-free investigation of molecular chemical compounds in gaseous, liquid or solid form, providing information about their functional groups or structure and thus enabling molecule-specific detection. The dominant technique in this field is Fourier transform infrared (FTIR) spectroscopy, which is routinely used for quantitative and qualitative analysis of infrared absorption spectra, including obtaining IR spectra of proteins.

The amide group -CONH- of the peptide bond is a primary source of fundamental vibrations, giving rise to nine characteristic absorption bands (amide A, amide B, and amides I–VII) in the infrared spectrum of proteins. Among them, the amide I band is the most prominent and the most frequently used for structural investigations [1]. The amide I band (1600–1700 cm^{-1}) arises mainly from C = O stretching vibrations, with minor contributions from NH in-plane bending and CN stretching [2]. Secondary structures of proteins can take different geometrical orientations (i.e., α-helices, β-sheets, turns, and random structures) depending on the local composition of the polyamide chain. These structures are stabilized by characteristic hydrogen bonding patterns involving C = O and N-H groups, which give the amide I band its distinctive band shapes and maxima positions, which are strongly related to secondary structure components of the protein. Detailed analysis of these band parameters using derivatives, curve-fitting, or deconvolution

#403981 https://doi.org/10.1364/OE.403981
Journal © 2020 Received 28 Jul 2020; revised 8 Oct 2020; accepted 20 Oct 2020; published 18 Nov 2020

Optics EXPRESS

techniques can reveal information regarding the type and proportion of secondary structures within a protein.

The main limitation of infrared investigations of proteins in aqueous solutions is associated with an intense absorption band originating from HOH bending vibrations, which is located around 1640 cm^{-1} and overlaps with the amide I band. Consequently, IR measurements in highly absorbing media must utilize very short sample-light interaction path lengths (3-8 μm for conventional FTIR spectrometers) [3]. Due to this experimental limitation, IR investigations of proteins are often performed in deuterium oxide (D_2O), as the DOD bending vibration is located near 1200 cm^{-1} and thus does not overlap with the spectral region of interest. As a result of this shift of solvent absorption, the use of heavy water allows increased path lengths, thereby improving the sensitivity of protein IR measurements. When working in deuterated solution, the amide I band shows a shift of 5–10 cm^{-1} to lower wavenumbers and is then referred to as the amide I' band [3–5].

Recent improvements in IR light-source technology led to the introduction of the quantum cascade laser (QCL). This powerful, polarized, and coherent source of mid-IR radiation opened new possibilities and approaches for chemical sensing schemes and triggered advancements in mid-IR spectroscopy [6]. In this context, QCLs may be considered the key technology for a new generation of highly selective and sensitive physical chemosensors [7]. The term physical chemosensor was coined by Vellekoop and refers to a type of sensor that measures physical parameters of a sample to derive chemical information [8]. In this respect, mid-IR spectroscopy in general, and QCL-based devices in particular, are promising candidates for the development of such sensors.

The broad spectral tunability of external cavity QCL (EC-QCL), typically over 200 cm^{-1}, has evoked growing interest in their application to broadband liquid-phase sensing. To date, such research has predominantly focused on performing absorption spectroscopy for analysis of liquids in transmission mode, reporting an improved detection of numerous analytes, including biological samples [9,10]. In the present work, hereafter the term absorption spectroscopy will be used to refer to the group of methods calculating the absorbance from measured transmittance [11]. A number of studies involving EC-QCL for broadband absorption spectroscopy of proteins in transmission mode have been carried out, leading to improved detection over conventional FTIR spectroscopy [12]. The use of high-power QCL sources led to a 4–5× increase in transmission path length, experimentally facilitating protein studies in highly absorbing aqueous solutions [13,14]. Other studies using EC-QCL have enabled secondary structure analysis of proteins at low concentrations in aqueous solution (>0.1 mg mL^{-1}) [15] and in deuterated solution (>0.25 mg ml^{-1}) [16], quantitative analysis of proteins in bovine milk samples [17–20], and monitoring of dynamic changes in protein secondary structure as a response to different types of external perturbations (e.g., pH, temperature, and chemical denaturation) [16,21,22].

The use of QCL sources in custom-made setups has significantly enhanced the robustness and variety of methods for mid-IR sensing. Nevertheless, laser-based absorption spectroscopy is sensitive to beam intensity fluctuations typically associated with high-intensity laser sources, contributing to noise and possibly limiting the dynamic range of detectors [23].

However, the unique properties of QCLs allow the realization of novel sensing schemes and experimental approaches. In this regard, measurements of the changes in refractive index (dispersion) rather than absorption of the investigated molecules is an approach that can harness the opportunities offered by QCLs while avoiding problems associated with laser-based absorption spectroscopy. Thus, refractive index sensing can (i) offer a high dynamic range for chemical detection, (ii) obtain background-free spectra, and (iii) be decoupled from pulse-to-pulse intensity fluctuations tied to QCL-based absorption spectroscopy. Absorption and dispersion are caused by the same process, a process that leads to attenuation of the radiation intensity and a phase shift upon passing through a sample. Hence, the same spectral information about a sample can

Optics EXPRESS

be retrieved by determining either absorption or dispersion. Due to this interconnection, the qualitative and quantitative evaluation of spectroscopic data based on the Lambert-Beer law can be, after careful consideration of its preconditions and limitations, applied to refractive index sensing [24,25]. A theoretical description of the relation between dispersion and absorption, i.e., real part n and imaginary part κ of the complex refractive index, is given by the Kramers-Kronig transformation (KKT) [26].

Dispersion spectroscopy measures the phase shift of light upon passing through the sample. The majority of current implementations for dispersion sensing are based on coherent laser sources and interferometric detection. Chirped laser dispersion spectroscopy (CLaDS) [23,27], the relatively new heterodyne phase-sensitive dispersion spectroscopy (HPSDS) [28], and interferometric cavity-assisted photothermal spectroscopy (ICAPS) [29] are three reported techniques for refractive index sensing using QCLs in gas-phase samples. For analysis of liquid-phase samples, a proof-of-principle setup based on an EC-QCL integrated in a Mach-Zehnder interferometer (MZI) for simultaneous acquisition of dispersion and absorbance mid-IR spectra in transmission has been demonstrated [30]. Subsequently, a slightly adapted setup was used to investigate liquid samples (in this case, sugars) to demonstrate the ability of dispersion spectroscopy to tackle challenging analytical problems [31]. However, the demonstration of dispersion spectroscopy as a fast, robust, and reliable detection scheme that can compete with well-established absorbance spectroscopy is still pending.

In this study, we present a fast and high-resolution mid-IR dispersion spectroscopy sensor for investigating liquid-phase samples and demonstrate its application to detection of proteins. A custom-made EC-QCL based Mach-Zehnder interferometer setup is employed to record dispersion and absorption spectra of multiple proteins with varying secondary structures. To the best of our knowledge, this is the first report on protein secondary structure analysis by refractive index sensing. Qualitative and quantitative analysis of different proteins was performed and the results compared to those obtained via FTIR spectroscopy. Finally, multivariate analysis of a ternary protein mixture is performed.

2. Experimental section

2.1. Reagents and samples

Heat-shock fraction of bovine serum albumin (≥98%), lyophilized powders of albumin from chicken egg white (≥98%), and concanavalin A from Jack bean (Type IV) were purchased from Sigma-Aldrich (Steinheim, Germany). Individual stock solutions of respective proteins were prepared and diluted in deuterium oxide (99.9 atom % D, Sigma-Aldrich) to five concentrations ranging from 0.25 to 2 mg mL^{-1}.

2.2. Experimental setup for dispersion spectroscopy

The experimental QCL-based Mach Zehnder interferometer setup employed for dispersion spectroscopy of proteins is depicted in Fig. 1. A thermoelectrically cooled external-cavity quantum cascade laser (Hedgehog, Daylight Solutions Inc., San Diego, CA), tunable from 1730 to 1470 cm^{-1}, was operated in pulse mode at a modulation frequency of 800 kHz and a duty cycle of 20%. A mesh was introduced to reduce the intensity of the emitted laser light, thus preventing detector saturation and ensuring linear response. The attenuated p-polarized beam was further split at a ratio of 50:50 (R:T) by a CaF_2 beam splitter (Thorlabs BSW510). One of the mirrors in the interferometer is attached to a piezo actuator (3.6 µm maximum displacement) connected to a commercial piezo controller (Thorlabs MDT694A), allowing precise adjustment of the interferometer beam paths prior to the measurement procedure. The transmitted and the reflected beam pass a temperature-stabilized (22.5 °C) transmission flow cell placed in the path of each of the beams with a 270 µm PTFE spacer between 1-in. CaF_2 wedged windows. The

Optics EXPRESS

beams are then recombined by a second identical beam splitter and focused by two parabolic gold mirrors (Thorlabs MPD229M01) on two thermoelectrically (TE) cooled HgCdTe (MCT) detectors operating at −78 °C (PVI-4TE-10.6, Vigo Systems S.A., Poland; detectivity: ≥2.0×10^9 cm Hz$^{1/2}$/W at 10.6 µm, window: wedged AR-coated ZnSe). The recorded detector signals were processed and digitized by a lock-in amplifier (MFLI, Zurich Instruments AG, Zurich, Switzerland) with an extended cut-off range of 5 MHz, equipped with the LabOne control software. The signals from the two channels were extracted by an in-house developed Python script (Python 3.7). All optical components of the setup were placed on a water-cooled breadboard (Thorlabs MBC3045/M) combined with a liquid cooling system (ThermoCube Liquid-to-Liquid, Solid State Cooling Systems) for enhanced temperature control and stabilization of the setup components and internal environment. The setup was sealed and purged with dry air before starting the measurements to minimize negative effects of water vapor bands in the investigated spectral region.

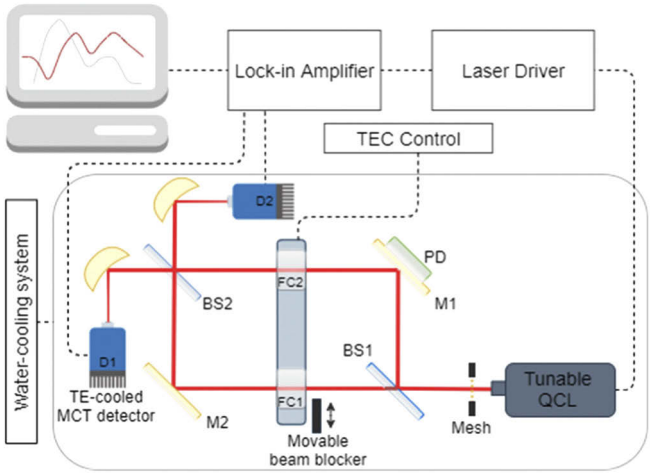

Fig. 1. Schematic of an EC-QCL-based Mach-Zehnder interferometer setup for dispersion spectroscopy of proteins.

2.3. Spectra acquisition

The experimental setup allows recording of both absorption and dispersion spectra in the spectral region defined by the tuning range of the laser. Dispersion spectra were recorded while the piezo actuator was held in position. The employed measuring approach features neither moving parts nor potential hysteresis [31] and consequently can be used for rapid spectra acquisition. Generally, spectra acquisition is based on the analysis of the differential detector signal $\Delta I_{\mathrm{rel}}(v)$ over the course of spectral scanning:

$$\Delta I_{rel}(v) = \frac{I_{D1} - I_{D2}}{I_{D1} + I_{D2}} \approx \sin\left(\frac{2\pi d}{\lambda}\Delta n\right). \tag{1}$$

Prior to the measurement, the differential signal was adjusted to 0 at 1600 cm^{-1} (mid-wavenumber of the spectral range), when both flow cells were filled with reference solution (solvent). The relation $\Delta I_{\mathrm{rel}}(v) = 0$ indicates an equal distribution of the intensity on both detectors. The adjustment to the zero-point was made by manually changing the voltage on the piezo-controller, driving the piezo-actuator and thus displacing the mirror mounted on the piezo element. After adjustment, background spectra (FC1: solvent, FC2: solvent) and sample spectra

Optics EXPRESS

(FC1: solvent, FC2: sample) were recorded. The presence of sample solution in one of the arms causes a phase shift and thus variations of the differential signal proportional to the refractive index of the sample. To obtain a dispersion spectrum of the sample, the background measurement was subtracted from the sample measurement, resulting in the analyte spectrum of the relative intensity $\Delta I_{\mathrm{rel}}(\nu)$. To derive the values of the relative change of the refractive index $\Delta n(\nu)$ from the measurement data, Eqs. (2) and (3) were applied. First, the spectrum of displacement $\delta(\nu)$ is calculated and then a spectrum of the sample's refractive index is derived.

$$\delta(\nu) = \frac{\lambda}{2\pi}\sin^{-1}[\Delta I_{rel}(\nu)], \tag{2}$$

$$\Delta n(\nu) = n - n_0 = \frac{\delta(\nu)\cdot\sqrt{2}}{d}. \tag{3}$$

Absorbance spectra were measured by blocking the beam in one of the arms of the interferometer with a movable shutter. The total amount of light transmitted through one flow cell filled with solution was measured by summing up the intensity recorded by the two detectors. Measurements were made for solvent and sample solutions and the absorbance spectrum was calculated as follows:

$$A(\nu) = -\log_{10}\left(\frac{I_{D1sample} + I_{D2sample}}{I_{D1solvent} + I_{D2solvent}}\right). \tag{4}$$

All obtained sample spectra were consecutively recorded to a common background spectrum.

2.4. Data processing

Protein dispersion and absorbance spectra were recorded with high resolution ($\leq$0.4 cm^{-1}; >7000 data points per scan) and high scan speed (3600 cm^{-1} s^{-1}) in the spectral region between 1470 and 1730 cm^{-1}. Three hundred scans were averaged per spectrum, with a total acquisition time of 45 s. Deviating scans originating from acquisition errors with a similarity index below 0.95 were eliminated [14]. The spectra were wavenumber-calibrated using the absorption bands of water vapor in order to reduce wavenumber deviations caused by inaccuracies introduced by the EC-QCL. The recorded IR spectra were filtered using a fast Fourier transform (FFT) filter with a cut-off frequency of 2500 Hz, yielding a spectral resolution of 1.5 cm^{-1}. Kramers-Kronig transformation of absorbance spectra was performed by an in-house-written script based on relations given in [26]. Quantitative evaluation of the comparability of the MZI measured (s_2) and FTIR reference (s_1) spectra was performed by calculating the degree of spectral overlap (s_{12}) utilizing the following expression:

$$s_{12} = \frac{||s_1^T s_2||}{||s_1||||s_2||}. \tag{5}$$

Data processing and spectra acquisition were performed with an in-house-developed MATLAB 2017a script.

2.5. FTIR measurements

FTIR absorption measurements were performed on a Vertex 80v FTIR spectrometer (Bruker Corp., Ettlingen, Germany) equipped with a liquid nitrogen cooled MCT detector (D* = 4.0×10^{10} cm Hz$^{1/2}$/W at 9.2 µm). Samples were measured in a transmission cell having CaF_2 windows and a 52 µm PTFE spacer. A total of 100 scans were averaged per spectrum, corresponding to an overall acquisition time of ~45 s. Spectra were recorded with a spectral resolution of 2 cm^{-1} and an aperture size of 2 mm and were calculated using a Black-Harris 3-term apodization function and zero filling factor of 2. The sample compartment of the FTIR instrument was purged with dry air prior to and during spectrum acquisition. Spectra were analyzed with OPUS 7.2 software package (Bruker Corp., Ettlingen, Germany).

Optics EXPRESS

3. Results and discussion

3.1. Qualitative analysis of protein dispersion spectra

The developed EC-QCL-based MZI setup is able to record refractive index spectra as well as absorbance spectra of proteins due to its dual capabilities and sensitivity to both optical properties κ and n. To demonstrate the capabilities of the developed sensor, three model proteins with significantly different secondary structures were chosen. Figure 2 shows the dispersion and absorbance spectra acquired by the introduced sensor. Concanavalin A (ConA), a protein predominantly containing β-sheets, shows a distinctive amide I' band with a maximum at 1636 cm^{-1} and a characteristic sideband at 1693 cm^{-1} in the absorbance spectrum [32,33]. Bovine serum albumin (BSA) is mainly composed of α-helix structures and gives rise to a broad amide I' band with a maximum located at 1648 cm^{-1} in deuterated solution [34]. Ovalbumin (Ova) consists of a mixture of α-helices and β-sheets in equal shares, resulting in a band maximum at 1640 cm^{-1} and a major shoulder at 1654 cm^{-1} [35]. The amide I' band position and shape of the measured MZI absorbance spectra show excellent comparability with spectra acquired via

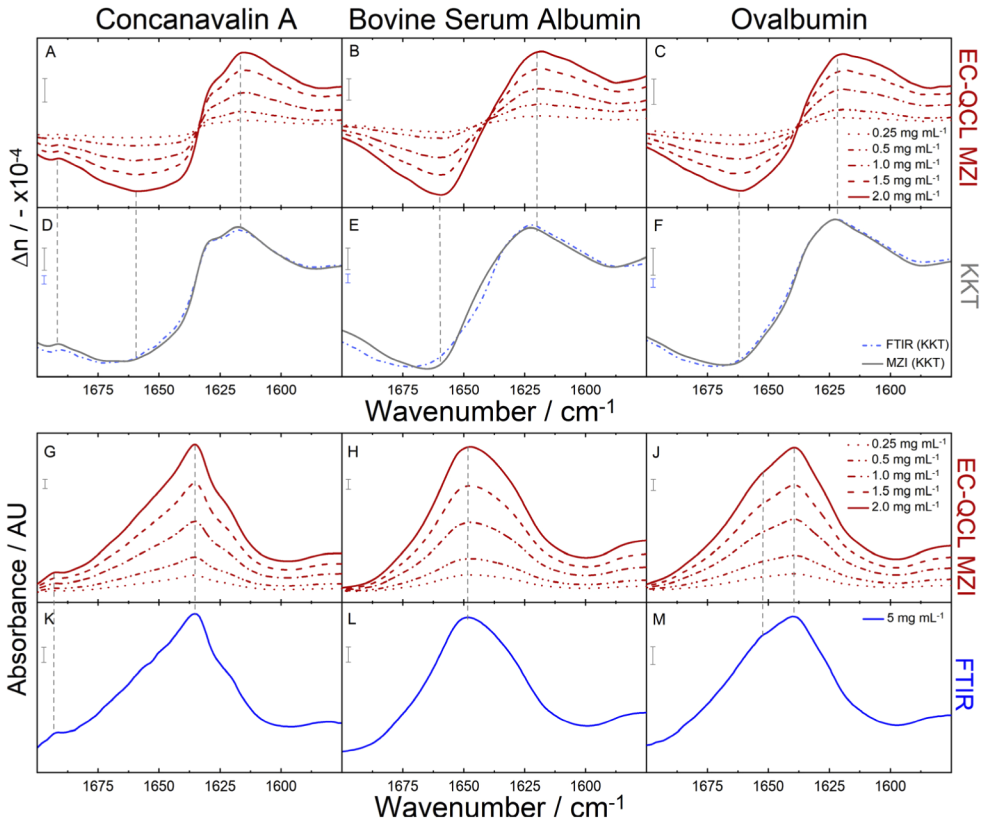

Fig. 2. (A–C) Measured IR dispersion spectra of proteins obtained by the EC-QCL MZI sensor in the concentration range of 0.25–2 mg mL^{-1}. (D–F) Calculated IR dispersion spectra of proteins by the Kramers-Kronig relations from FTIR absorbance spectrum of 5 mg mL^{-1} (dashed blue line) and from MZI absorbance spectrum for 2 mg mL^{-1} (gray solid line). (G–J) IR absorbance spectra of proteins recorded by the EC-QCL MZI sensor in the concentration range of 0.25–2 mg mL^{-1}. (K–M) FTIR absorbance spectra of proteins with concentration of 5 mg mL^{-1}. Gray bars indicate the dispersion of 1×10^{-4} and absorbance of 10 mAU.

Optics EXPRESS

FTIR spectroscopy. To highlight the high conformance between the MZI and FTIR absorbance spectra, the degree of spectral overlap s_{12} was evaluated; all three protein spectra showed overlap of >0.999. The recorded dispersion spectra of the proteins are depicted in Fig. 2(A)–2(C). Their shape shows the characteristic behavior of anomalous dispersion (i.e., $\delta n/\delta \nu<0$) of the refractive index function in the vicinity of an absorbance band. Furthermore, even small spectral features, such as the sideband of ConA at 1693 cm^{-1}, are very well represented in the measured refractive index spectra. Analysis of the positions and shape of the spectral regions showing anomalous dispersion allow distinction between proteins with different secondary structures in a similar—although not as straightforward—fashion to analysis of band maxima in absorbance spectra. Direct comparison of the spectra obtained for the three proteins is shown in Supplement 1, Fig. S1. Due to the lack of a reference analytical technique for broadband dispersion spectroscopy in the mid-IR region, the experimentally obtained dispersion spectra were validated against the theoretical KK-transformed FTIR absorbance spectra (Fig. 2(D)–2(F)). Furthermore, the MZI-acquired absorbance spectra also underwent KK transformation for additional verification. The shape of the measured dispersion spectra agrees very well with the KK-transformed FTIR absorbance spectra. The degree of spectral overlap for the normalized refractive index spectra was $s_{12} > 0.98$. Small deviations from the calculated spectrum are expected as the chosen spectral acquisition method does not require moving parts. Here, the theoretical derivation of $\Delta I_{\mathrm{rel}}(\nu)$ includes the approximation $A \approx 0$, which is not fully met, thus introducing small shape deformations in experimental measurements [31].

3.2. Quantitative analysis

For quantitative analysis, the recorded refractive index spectra of the proteins were evaluated along the region of anomalous dispersion, coinciding with the amide I' band region in the absorbance spectra. To this end, the amplitude of the Δn function between the local minima and maxima next to the inflection point was evaluated and employed for calibration (Supplement 1, Fig. S2). The calibration curves confirm the expected high linearity ($R^2 > 0.999$) of the refractive index function with concentration (Supplement 1, Fig. S3). Moreover, this assessment method is highly robust against potential offsets which might occur due to manual liquid handling. For comparison, absorbance spectra of proteins were evaluated using the heights of the amide I' band maxima.

Utilization of a powerful EC-QCL in the MZI setup enables use of longer transmission paths (~5×) than in FTIR spectroscopy, leading to generally higher absorption bands and thus sensitivity. Figures of merit obtained for quantitative analysis of the sensor performance for the detection of proteins are summarized in Table 1. Regarding absorbance spectroscopy, the noise level achieved by the MZI sensor is similar to that achieved with a commercial high-end FTIR spectrometer, even though the detectivity of the TE-cooled MCT detectors used herein is 20 times lower. Consequently, due to higher sensitivity at the same noise level, lower limit of detection (LOD) could be achieved for MZI absorbance measurement and the LOD of the dispersion measurement was in the same order of magnitude as that for FTIR spectroscopy. Finally, in order to quantitatively compare the quality of the two analytical methods for protein sensing (absorbance vs. dispersion), standard deviations of the methods, S_{xo} (details in Supplement 1), were evaluated and found to be nearly identical for absorbance and refractive index spectra.

The obtained quantitative figures of merit show that the presented method for refractive index sensing compares favorably with conventional absorbance spectroscopy, delivering similar results; both techniques can be equivalently used for qualitative as well as quantitative protein analysis.

3.3. Multivariate quantification of protein mixtures

To showcase the potential of dispersion spectroscopy to tackle complex analytical problems, multivariate quantification of ternary protein solutions via application of partial least squares

Optics EXPRESS

Table 1. Comparison of the quantitative results obtained for dispersion and absorption spectroscopy of proteins on the example of bovine serum albumin using the EC-QCL MZI sensor and FTIR.

	Dispersion MZI	Absorbance MZI	FTIR
R^2	> 0.999	> 0.999	> 0.999
Sensitivity (AU mL mg^{-1})	$3.4 \cdot 10^{-4}$	$7.4 \cdot 10^{-2}$	$1.8 \cdot 10^{-2}$
Noise$_{RMS}$ (-/AU)	$8.0 \cdot 10^{-7}$	$1.6 \cdot 10^{-5}$	$1.3 \cdot 10^{-5}$
LOD (mg mL^{-1})	0.0070	0.0007	0.0022
S_{xo} (mg mL^{-1})	0.013	0.015	0.012

(PLS) regression models was performed. Simultaneous quantification of multiple proteins in IR absorption spectra by PLS is routinely performed [18,20,36], thus posing an excellent problem for benchmarking the performance of the developed sensor. A calibration dataset consisting of 15 samples was prepared containing mixtures of the three proteins (ConA, BSA, and Ova) in D_2O in the concentration range of 0.1 to 2 mg mL^{-1}. Dispersion and absorbance spectra were recorded by the EC-QCL-based MZI setup and the obtained data set was subjected to PLS modelling (PLS Toolbox 8.8.1, Eigenvectors Research Inc.). Identical data pretreatment tools were used for both spectra types to ensure accurate comparison. Furthermore, the analyzed spectral range was restricted to the amide I' region (1590–1710 cm^{-1}). To improve the quality of the calibration models, spectra were preprocessed via mean centering and derivative transformations, with additional smoothing using a Savitzky-Golay filter. To avoid overfitting, the optimal number of latent variables in the model was determined by leave-one-out cross-validation. Table 2 shows the PLS calibration parameters and internal figures of merit. Coefficients of determination (R^2) of calibration are >0.988 and >0.990 for dispersion and absorption spectra, respectively, indicating excellent calibration. The root-mean-square error of calibration (RMSEC) and cross-validation (RMSCV) for individual proteins span between 0.030–0.061 mg mL^{-1} and 0.047–0.114 mg mL^{-1} for dispersion, and 0.022–0.058 mg mL^{-1} and 0.031–0.095 mg mL^{-1} for absorbance spectra. The bias of cross-validation (CV bias) as a measure of accuracy was not greater than 0.007 and 0.003 mg mL^{-1}, respectively, for dispersion and absorbance spectra. Slightly worse performance of the PLS models for ovalbumin in both spectroscopy types was related to its highly overlapping spectral features. Overall, the obtained figures of merit for dispersion spectra of proteins compare very well with those obtained for absorbance spectra, demonstrating the potential of dispersion spectroscopy utilizing the developed sensor to quantify mixtures of multiple proteins with different secondary structures.

3.4. Experimental measures to enable low-noise MZI dispersion spectroscopy

In the setup described, use of a latest generation EC-QCL featuring fast tuning speeds and MCT detectors enabled rapid spectra acquisition. This significantly reduced the impact of low frequency noise (drifts) caused by external environmental factors. Compared to an earlier prototype of the sensor [31], the acquisition rates were improved from 1 cm^{-1}/s to 3600 cm^{-1}/s, allowing spectral averaging. Further, the high spectral resolution (≤0.4 cm^{-1}) of the recorded data allows minor filtering of the refractive index spectra. These factors reduce noise levels compared to FTIR spectra at similar acquisition times.

Another important measure permitting stable and sensitive refractive index sensing was the implementation of rigorous temperature control in the setup. This step is necessary due to the delicate nature of interferometric measurements. Firstly, the optical components were placed on a water-cooled breadboard, decoupling it from the effects of ambient temperature drift and preserving the measuring zero-point over multiple days. The need for fine readjustments of

Optics EXPRESS

Table 2. PLS calibration parameters and internal figures of merit.[a]

	Dispersion spectra			Absorption spectra		
	ConA	BSA	Ova	ConA	BSA	Ova
Concentration range (mg mL^{-1})	0.1-2.0			0.1-2.0		
Preprocessing	MC, 2nd Der.	MC, 2nd Der.	MC, 2nd Der.	MC, 2nd Der.	MC, 2nd Der.	MC, 2nd Der.
LVs	3	3	4	3	3	4
Exp. Var. (%)	98.52	98.52	99.04	99.86	99.86	99.98
RMSEC (mg mL^{-1})	0.032	0.030	0.061	0.022	0.032	0.058
RMSECV (mg mL^{-1})	0.047	0.054	0.114	0.031	0.048	0.095
R^2 Cal	0.997	0.997	0.988	0.999	0.997	0.990
R^2 CV	0.994	0.992	0.960	0.997	0.994	0.972
CV Bias (mg mL^{-1})	0.001	0.003	0.007	0.001	0.003	0.001

[a]MC: mean centering, 2nd Der: second derivative calculated using Savitzky-Golay filter (order: 2, window 381 points/15 cm^{-1}), R^2: coefficient of determination, Cal: calibration; CV: cross validation; RMSEC: root-mean-square error of calibration, RMSECV: root-mean-square error of cross-validation, LVs: latent variable(s).

the interferometric arms was reduced to ±0.12 to 0.24 µm in day-to-day operation. Secondly, additional temperature stabilization was integrated in the transmission flow cell and controlled by a TEC to regulate the temperature of the sample along the transmission path length (270 µm), preventing temperature-related offsets between solvent and sample measurement. Approximately 60 to 90 seconds were needed to stabilize the temperature of the solution after injection, ensuring long-term repeatability of recorded spectra.

Reproducible sample handling also plays an important role in this sensitive interferometric method. Manual injection is inherently associated with pronounced pressure variations on the flow cell windows, causing changes of the transmission path length, resulting in offsets or even deformations in the recorded ΔI_{rel} signal. Offsets corresponding to a change of transmission path length of ±0.6 µm were observed during test measurements. In this context, it was found that integration of an automated injection system ensured constant pressure during each injection event, minimizing this negative effect.

Finally, when working in the challenging mid-IR spectral region, where water vapor absorption occurs, placing the sensor in a closed housing that is constantly purged with dry air is critical to reducing overall noise.

4. Conclusions

In summary, we presented an innovative custom-made Mach-Zehnder interferometer-based sensor for dispersion spectroscopy of proteins. This is also the first time refractive index spectra of proteins have been measured across such a wide spectral range and at such high speed and resolution. We demonstrated that refractive index sensing can be successfully used to derive qualitative and quantitative information from liquid-phase samples. Furthermore, the developed sensor can record both broadband absorption and dispersion spectra, allowing internal comparison and referencing. The measured refractive index spectra of proteins showed good agreement with Kramers-Kronig transformed FTIR absorbance spectra. We further demonstrated that laser-based dispersion spectroscopy achieves figures of merit similar to those of established high-end FTIR spectroscopy at similar acquisition times.

The slightly higher LOD obtained for dispersion spectroscopy can be explained by the higher sensitivity to external factors of the interference-based approach. Application of extensive temperature control minimized the associated problems and significantly improved the setup stability and repeatability. These control measures enabled us to obtain measurements of

Optics EXPRESS

refractive index fluctuations with accuracy down to 10^{-7}, which is currently considered the experimental limit for interferometry in a free-space setup operated under ambient conditions [37,38].

Potential future improvements of this sensor include construction of a custom-made transmission cell that can counter the effects of optical path length change upon each injection, which negatively affects the measurement sequence. Furthermore, the method described here involves a fixed piezo element, which suffers from the lack of a measured physical unit (mirror displacement is only calculated) and sensitivity to laser fluctuations. Planned developments of the sensor for liquid-phase dispersion spectroscopy include the implementation of fast, hysteresis-free phase-locked interferometric detection and miniaturization of the sensor.

We believe that further development of this novel EC-QCL-based MZI sensing scheme for refractive index sensing in liquid-phase samples can eventually leverage all the advantages of dispersion spectroscopy and outperform traditional absorbance sensing techniques.

Funding

Austrian Science Fund FWF (P32644-N); Horizon 2020 Framework Programme (780240).

Disclosures

The authors declare no conflicts of interest.

See Supplement 1 for supporting content.

References

1. B. Stuart, *Infrared Spectroscopy: Fundamentals and Applications* (John Wiley & Sons, Ltd, 2004).
2. ÁI López-Lorente and B. Mizaikoff, "Mid-infrared spectroscopy for protein analysis: Potential and challenges," Anal. Bioanal. Chem. **408**(11), 2875–2889 (2016).
3. H. Fabian and W. Mäntele, "Infrared Spectroscopy of Proteins," in *Handbook of Vibrational Spectroscopy*, J. M. Chalmers, ed. (John Wiley & Sons, Ltd, 2006).
4. A. Barth and C. Zscherp, "What vibrations tell us about proteins," Q. Rev. Biophys. **35**(4), 369–430 (2002).
5. ÁI López-Lorente, P. Wang, and B. Mizaikoff, "Towards label-free mid-infrared protein assays: In-situ formation of bare gold nanoparticles for surface enhanced infrared absorption spectroscopy of bovine serum albumin," Microchim. Acta **184**(2), 453–462 (2017).
6. A. Schwaighofer, M. Brandstetter, and B. Lendl, "Quantum cascade lasers (QCLs) in biomedical spectroscopy," Chem. Soc. Rev. **46**(19), 5903–5924 (2017).
7. R. F. Curl, F. Capasso, C. Gmachl, A. A. Kosterev, B. McManus, R. Lewicki, M. Pusharsky, G. Wysocki, and F. K. Tittel, "Quantum cascade lasers in chemical physics," Chem. Phys. Lett. **487**(1-3), 1–18 (2010).
8. M. J. Vellekoop, "Physical Chemosensors," in *Smart Sensor Systems*, G. C. M. Meijer, ed. (John Wiley & Sons, 2008), pp. 121–150.
9. M. Brandstetter, L. Volgger, A. Genner, C. Jungbauer, and B. Lendl, "Direct determination of glucose, lactate and triglycerides in blood serum by a tunable quantum cascade laser-based mid-IR sensor," Appl. Phys. B **110**(2), 233–239 (2013).
10. M. Brandstetter, A. Genner, K. Anic, and B. Lendl, "Tunable external cavity quantum cascade laser for the simultaneous determination of glucose and lactate in aqueous phase," Analyst **135**(12), 3260–3265 (2010).
11. T. G. Mayerhöfer, H. Mutschke, and J. Popp, "Employing theories far beyond their limits—The case of the (Boguer-) Beer–Lambert Law," ChemPhysChem **17**(13), 1948–1955 (2016).
12. A. Schwaighofer and B. Lendl, "Quantum cascade laser-based infrared transmission spectroscopy of proteins in solution," in *Vibrational Spectroscopy in Protein Research* (Elsevier, 2020), pp. 59–88.
13. M. R. Alcaráz, A. Schwaighofer, C. Kristament, G. Ramer, M. Brandstetter, H. Goicoechea, and B. Lendl, "External-cavity quantum cascade laser spectroscopy for mid-IR transmission measurements of proteins in aqueous solution," Anal. Chem. **87**(13), 6980–6987 (2015).
14. A. Schwaighofer, M. Montemurro, S. Freitag, C. Kristament, M. J. Culzoni, and B. Lendl, "Beyond Fourier Transform infrared spectroscopy: External cavity quantum cascade laser-based mid-infrared transmission spectroscopy of proteins in the amide I and amide II region," Anal. Chem. **90**(11), 7072–7079 (2018).

Optics EXPRESS

15. C. K. Akhgar, G. Ramer, M. Żbik, A. Trajnerowicz, J. Pawluczyk, A. Schwaighofer, and B. Lendl, "The next generation of IR spectroscopy: EC-QCL based mid-IR transmission spectroscopy of proteins with balanced detection," Anal. Chem. **92**(14), 9901–9907 (2020).
16. A. Schwaighofer, M. R. Alcaráz, C. Araman, H. Goicoechea, and B. Lendl, "External cavity-quantum cascade laser infrared spectroscopy for secondary structure analysis of proteins at low concentrations," Sci. Rep. **6**(1), 33556–10 (2016).
17. J. Kuligowski, A. Schwaighofer, M. R. Alcaráz, G. Quintás, H. Mayer, M. Vento, and B. Lendl, "External cavity-quantum cascade laser (EC-QCL) spectroscopy for protein analysis in bovine milk," Anal. Chim. Acta **963**, 99–105 (2017).
18. A. Schwaighofer, J. Kuligowski, G. Quintás, H. K. Mayer, and B. Lendl, "Fast quantification of bovine milk proteins employing external cavity-quantum cascade laser spectroscopy," Food Chem. **252**, 22–27 (2018).
19. A. Schwaighofer, M. R. Alcaráz, J. Kuligowski, and B. Lendl, "Recent advancements of EC-QCL based mid-IR transmission spectroscopy of proteins and application to analysis of bovine milk," Biomed. Spectrosc. Imaging **7**(1-2), 35–45 (2018).
20. M. Montemurro, A. Schwaighofer, A. Schmidt, M. J. Culzoni, H. K. Mayer, and B. Lendl, "High-throughput quantitation of bovine milk proteins and discrimination of commercial milk types by external cavity-quantum cascade laser spectroscopy and chemometrics," Analyst **144**(18), 5571–5579 (2019).
21. A. Schwaighofer, M. R. Alcaraz, L. Lux, and B. Lendl, "pH titration of β-lactoglobulin monitored by laser-based mid-IR transmission spectroscopy coupled to chemometric analysis," Spectrochim. Acta, Part A **226**, 117636 (2020).
22. M. R. Alcaráz, A. Schwaighofer, H. Goicoechea, and B. Lendl, "EC-QCL mid-IR transmission spectroscopy for monitoring dynamic changes of protein secondary structure in aqueous solution on the example of β-aggregation in alcohol-denaturated α-chymotrypsin," Anal. Bioanal. Chem. **408**(15), 3933–3941 (2016).
23. M. Nikodem and G. Wysocki, "Molecular dispersion spectroscopy - new capabilities in laser chemical sensing," Ann. N. Y. Acad. Sci. **1260**(1), 101–111 (2012).
24. T. G. Mayerhöfer, A. Dabrowska, A. Schwaighofer, B. Lendl, and J. Popp, "Beyond Beer's Law: Why the index of refraction depends (almost) linearly on concentration," ChemPhysChem **21**(8), 707–711 (2020).
25. T. G. Mayerhöfer, S. Pahlow, and J. Popp, "The Bouguer-Beer-Lambert Law: Shining light on the obscure," ChemPhysChem **21**(18), 2029–2046 (2020).
26. G. Ramer and B. Lendl, "Attenuated total reflection Fourier transform infrared spectroscopy," Encycl. Anal. Chem. (2013).
27. G. Wysocki and D. Weidmann, "Molecular dispersion spectroscopy for chemical sensing using chirped mid-infrared quantum cascade laser," Opt. Express **18**(25), 26123–26140 (2010).
28. P. Martín-Mateos, J. Hayden, P. Acedo, and B. Lendl, "Heterodyne phase-sensitive dispersion spectroscopy in the mid-infrared with a quantum cascade laser," Anal. Chem. **89**(11), 5916–5922 (2017).
29. J. P. Waclawek, C. Kristament, H. Moser, and B. Lendl, "Balanced-detection interferometric cavity-assisted photothermal spectroscopy," Opt. Express **27**(9), 12183–12195 (2019).
30. J. Hayden, S. Hugger, F. Fuchs, and B. Lendl, "A quantum cascade laser-based Mach–Zehnder interferometer for chemical sensing employing molecular absorption and dispersion," Appl. Phys. B **124**(2), 29 (2018).
31. S. Lindner, J. Hayden, A. Schwaighofer, T. Wolflehner, C. Kristament, M. González-Cabrera, S. Zlabinger, and B. Lendl, "External cavity quantum cascade laser-based mid-infrared dispersion spectroscopy for qualitative and quantitative analysis of liquid-phase samples," Appl. Spectrosc. **74**(4), 452–459 (2020).
32. J. L. R. Arrondo, N. M. Young, and H. H. Mantsch, "The solution structure of concanavalin A probed by FT-IR spectroscopy," Biochim. Biophys. Acta (BBA)/Protein Struct. Mol. **952**, 261–268 (1988).
33. U. Novak and J. Grdadolnik, "The hydration of Concanavalin A studied by infrared spectroscopy," J. Mol. Struct. **1135**, 138–143 (2017).
34. J. Grdadolnik and Y. Maréchal, "Hydrogen-deuterium exchange in bovine serum albumin protein monitored by Fourier transform infrared spectroscopy, Part I: Structural studies," Appl. Spectrosc. **59**(11), 1347–1356 (2005).
35. A. Dong, J. D. Meyer, J. L. Brown, M. C. Manning, and J. F. Carpenter, "Comparative Fourier transform infrared and circular dichroism spectroscopic analysis of α1-proteinase inhibitor and ovalbumin in aqueous solution," Arch. Biochem. Biophys. **383**(1), 148–155 (2000).
36. S. Großhans, M. Rüdt, A. Sanden, N. Brestrich, J. Morgenstern, S. Heissler, and J. Hubbuch, "In-line Fourier-transform infrared spectroscopy as a versatile process analytical technology for preparative protein chromatography," J. Chromatogr. A **1547**, 37–44 (2018).
37. N. Bobroff, "Recent advances in displacement measuring interferometry," Meas. Sci. Technol. **4**(9), 907–926 (1993).
38. J. C. Owens, "Optical refractive index of air: Dependence on pressure, temperature and composition," Appl. Opt. **6**(1), 51–59 (1967).